Journal of Nuclear Materials 384 (2009) 175–189

Contents lists available at ScienceDirect

Journal of Nuclear Materials

journal homepage: www.elsevier.com/locate/jnucmat

Review

The aluminum chemistry and corrosion in alkaline solutions

Jinsuo Zhang *, Marc Klasky, Bruce C. Letellier

International Nuclear System Engineering, MS-K 575, Los Alamos National Laboratory, Los Alamos, NM 87545, United States

ARTICLE INFO

Article history:
Received 11 May 2008
Accepted 10 November 2008

ABSTRACT

Aluminum–alkaline solution systems are very common in engineering applications including nuclear engineering. Consequently, a thorough knowledge of the chemistry of aluminum and susceptibility to corrosion in alkaline solutions is reviewed. The aluminum corrosion mechanism and corrosion rate are examined based on current experimental data. A review of the phase transitions with aging time and change of environment is also performed. Particular attention is given to effect of organic and inorganic ions. As an example, the effect of boron is examined in detail because of the application in nuclear reactor power systems. Methods on how to reduce the corrosion rate of aluminum in alkaline solutions are also highlighted.

Contents

1. Introduction

Aluminum and its alloys are widely used in many engineering applications and scientific technologies, such as in aerospace, advanced nuclear reactor, surface coating, metal/air batteries, etc. For example, aluminum–alkaline solution systems are often utilized in the development of metal/air batteries in which the aluminum is used as the anode. These batteries may be used as power sources for electric vehicle propulsion. The battery performance is determined by the electrochemical and corrosion properties of aluminum anodes [1]. Consequently, the aluminum behavior has an import impact on the battery properties. Another common example of aluminum–alkaline solution systems can be found in nuclear water reactors during a loss of coolant accident (LOCA). The chemical environment generated by the injection of coolant into the emergency-core-cooling-system has a pH around 10 [2]. The release of aluminum into solution via corrosion may result in precipitate, which may lead to a system failure.

* Corresponding author. Tel.: +1 505 667 7444; fax: +1 505 665 2897.
E-mail address: jszhang@lanl.gov (J. Zhang).

0022-3115/$ - see front matter © 2008 Elsevier B.V. All rights reserved.
doi:10.1016/j.jnucmat.2008.11.009

It is well known that aluminum oxide scale generally can provide better oxidation resistance and yield a lower oxidation rate than other protective oxide layers, for example chrome oxide scale. The aluminum oxide scale is compact and thermodynamically stable in neutral environments, and it also has a good adherence to the substrate. Therefore, the aluminum oxide scale appears to be an ideal protective scale. However, it has been reported that the scale can be dissolved and exists in the solution as the following species: Al^{+3}, $Al(OH)^{+2}$, $Al(OH)_2^+$ and $Al(OH)_4^-$, in an acidic or alkaline solution.

Because of the extensive applications, the behavior of aluminum and its alloys in various systems have been extensively studied. Critical review articles on the aluminum–water system have been performed by Alwitt [3] and on localized corrosion by Foley [4]. In the present study, we focus on the aluminum–alkaline systems. Available experimental data and theoretical analyses are organized and reviewed. The present studies lead to rethinking of the available data by theoretical and experimental studies.

The rests of the article are organized as following:

- Section 2 presents the aluminum hydroxide phases and the factors that affect the phase transition.
- Section 3 addresses the aluminum solubility in alkaline solution. Methods on how to predict the solubility are presented in this section.
- Section 4 presents the boron effects on aluminum behaviors in alkaline solution including aluminum–boron complex formation and the boron adsorption on aluminum hydroxide.
- Section 5 reviews the particle size distribution measurements of aluminum–alkaline system.
- Section 6 addresses the aluminum corrosion in alkaline solution, including the corrosion mechanism, corrosion rate data, corrosion inhibition and film kinetics.
- Conclusions are summarized in Section 7.

2. Aluminum hydroxide

2.1. Hydroxide phases

In an aluminum–alkaline solution system, a determination of the dissociation of the aluminum hydroxide solid phase is needed in order to determine the solubility of aluminum in the solution. It has been reported that the dissolution process is a function of the aluminum hydroxide solid phase. The aluminum hydroxide may exist in an amorphous form or as one of three crystalline forms known as gibbsite, bayerite, or nordstrandite. The crystalline polymorphs differ only in the packing arrangement of the layers [5], and the Al–O–Al layer framework is identical [6]. Each aluminum ion has three neighboring Al coordinated with pairs of hydroxyl groups. The layers are held together by a network of hydrogen bounds. Ordering of these layers forms the essential difference between these structures. In gibbsite, the hydroxyl groups of one layer are stacked directly on top of the hydroxyl groups of the next layer, creating a crystal of hexagonal morphology, and their relationships are clearly of type AB–BA–AB as shown in Fig. 1. The hydroxyl groups of bayerite reside in the depressions of the layers below and above, creating a conically shaped crystal. The bayerite has an AB–AB type lattice. Nordstrandite also has an AB–AB type lattice and is composed of alternating layers of gibbsite and bayerite [6].

XRD has been utilized to characterize aluminum hydroxide crystalline structure. Gibbsite (α) is identified by the presence of three principal diffraction lines at 0.485, 0.437, and 0.432 nm. Bayerite (β) is distinguished by strong diffraction lines at 0.472 and 0.436 nm, whereas nordstrandite (γ) is detected by the presence of three major diffraction lines at 0.479, 0.433, and 0.422 nm. The amorphous precipitate produces a diffraction pattern that is only a halo around the range of 3–4 nm [7].

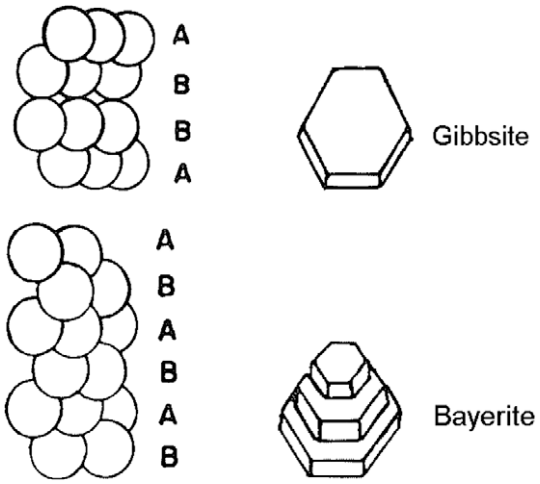

Fig. 1. Gibbsite and bayerite layer stacking patterns [5].

Two other common crystals that form in aluminum–alkaline solution are boehmite and pseudoboehmite with composition of AlOOH. These two crystals are built up out of the same fundamental: a double sheet of octahedral crystals with Al ions at their center, but there is a variable amount of water between double octahedral layers. The major distinction between pseudoboehmite and boehmite is that the former has broad diffraction peaks and that the spacing of the first peak of pseudoboehmite is larger than that of boehmite.

2.2. Phase transition

Numerous experiments have been conducted in alkaline systems on the phase transition of the solid aluminum hydroxide. These experiments were critically reviewed by Nordstrom and May [8]. It has been found that the equilibrium solid phases are a complex function of the experimental conditions and the nature of the materials utilized, i.e., particle size and surface area [8]. To address the sensitivity of the results to experimental conditions, an elaborate device in which acidified aluminum nitrate solutions were titrated with alkali (NaOH or KOH) was designed [9]. Considerable effort was devoted to ensuring vigorous mixing of the reactants so as to avoid local hydroxyl ion concentrations appreciably larger than the overall concentration, as this will result in the formation of a local precipitate.

Results from the investigation (Ref. [9]) are shown in Table 1. Clearly, the aluminum hydroxide solid phase formation is a function of temperature and pH. It was reported that visible precipitate in the system with an initial aluminum nitrate concentration of 0.072 M first occurred at approximately a pH 6.1 and 25 °C. Decrease in temperature leads to a lowering of the onset pH of solid phase formation. It should be noted that in these studies neither precipitate nor colloids were found at OH/Al ratios of less than 2.5, even after aging for 2 months. (The value of OH/Al = 2.5 is very close to the vector percolation threshold of 2.4, which represents the minimum number of cross links required for a 3-D structure to attain rigidity [6].) However, in more common investigations where the hydroxyl ion concentration is non-uniformly added, a different behavior is observed. Depending on the rate of alkali addition, the solid phase can be formed at OH/Al ratios of less than 2.5. In addition, the non-uniform addition of the alkali yields a more-crystalline product than the amorphous product that is found in a more uniform setting [10,11].

Table 1
Aluminum hydroxide solid phases as functions of pH and temperature [9].

pH	Temperature (°C)				
	24	28	40	60	90
6	A				A
7	Microbay		A	A	A
8	Microbay		A	A	
9	Microbay		A	A	Gellbo
10	Microbay ↓ Bay	Bay	A ↓ Bay	Microbay ↓ Bay ↓ Gibb	Gelbo (Gibb) (Bay)

A = amorphous; microbay = amorphous with few diffuse lines of bayerite; gibb = gibbsite; bay = bayerite; gellbo = gelatinous boehmite.

Table 2
Effect of age on the pH and crystalline structure of aluminum hydroxide prepared form 0.0378 M aluminum nitrate solution at 25 °C [12].

OH/Al	2.90	2.95	3.02	3.25
Initial pH	5.00	5.50	8.00	9.50
1 Day	4.85 Amorphous	5.48 Amorphous	7.85 Weak Pseudoboehmite	10.64 Mixed Pseudoboehmite/bayerite
1 Week	4.82 Amorphous	5.18 Amorphous	7.60 Mixed Pseudoboehmite/bayerite	10.74 Mixed Pseudoboehmite/bayerite/gibbsite
1 Month	4.29 Amorphous	4.35 Amorphous	7.50 Mixed Pseudoboehmite/bayerite	10.79 Mixture bayerite gibbsite
Heated (5 days)	4.05 Gibbsite	4.10 Gibbsite	7.25 Pseudoboehmite	9.47 Gibbsite

In another investigation of the phase behavior of aluminum hydroxide systems, Hayden [12] found that the phase transition was also dependent on aging and affects the pH. The results are presented in Table 2. The table shows that increasing the initial pH > 8 combined with aging lead to the appearance of a more-crystalline product. In addition, as may be seen at less than 9.5, aging has the effect of decreasing the pH. Furthermore, an increase in temperature in all cases decreases the pH. The observed change in pH is due to precipitation, and the formation of double hydroxide bridges which occurs by the sequential deprotonation and dehydration reactions shown below:

$$Al(OH2)_6^{3+} = Al(OH)(OH2)_5^{2+} + H^+, \quad (1)$$

$$Al(OH)(OH2)_5^{2+} = Al_2(OH)_2(OH2)_8^{4+} + 2H_2O. \quad (2)$$

Because it is generally accepted that under slight alkaline conditions the rate-limiting step in the precipitation of aluminum hydroxide is the formation of Al–OH–Al bridges, the ratio OH/Al is of paramount importance [13].

Table 2 also shows that the aluminum hydroxide precipitate recovered from aged solutions at OH/Al of 2.90 and 2.95 is amorphous when aged one month at 25 °C, but heating up to 65 °C for five days produces gibbsite. At an OH/Al ratio of 3.02, crystalline aluminum hydroxide consisting of bayerite and pseudoboehmite was found after aging one month. At an OH/Al ratio of 3.25, a mixture of pseudoboehmite and bayerite was identified much sooner in the solid phase. Heating of the solution prepared at OH/Al ratio of 3.02 and 3.25 for five days produced pseudoboehmite [12]. Therefore, the aluminum hydroxide phase transition depends strongly on OH/Al ratio as well as the aging temperature.

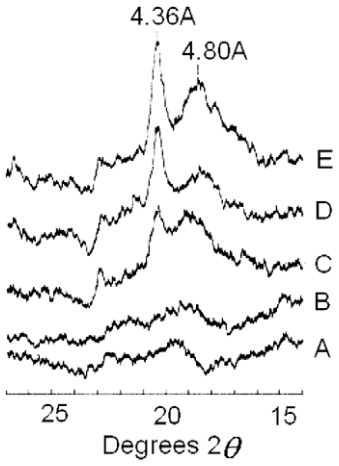

Fig. 2. Change in XRD pattern of aluminum hydroxide gel during aging at 25 °C for (A) 56 days, (B) 78 days, (C) 94 days, (D) 115 days, (E) 189 days [20].

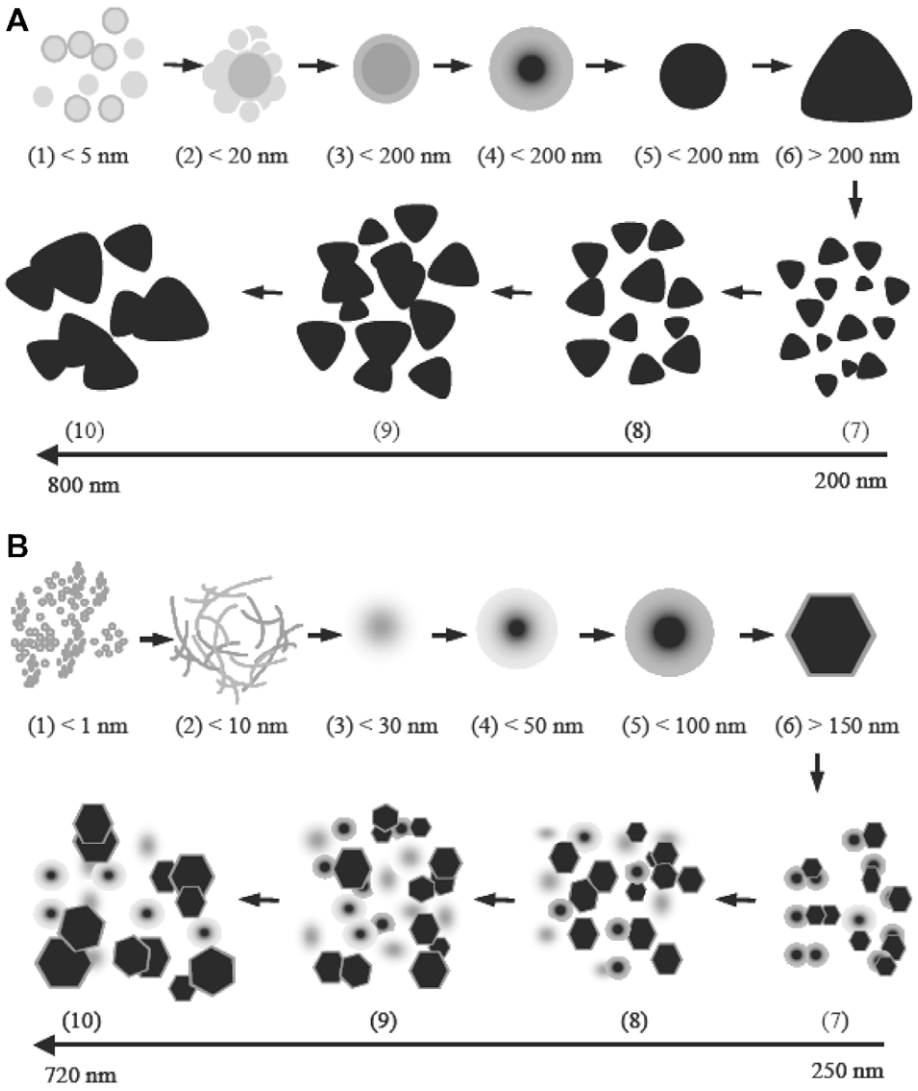

Fig. 3. A schematic representation of the formation and enlargement of crystalline aluminum hydroxide from sodium aluminate solutions. (A) Dilute solutions, (B) concentrated solutions. The size ranges indicated are speculative and are based on literature sources [21].

The phase transitions are related to the pH of solution and the concentration of aluminum in the solution. A criterion is defined by

$$X = -\log(c_{H^+}) - \log(c_{Al}), \quad (3)$$

where c is the concentration of element in M. Van Straten [10] reported that in cases where $X < 12$, the transition of phases as a function of aging is amorphous–pseudoboehmite–bayerite, whereas if $12 < X < 12.55$, the phase transition will be pseudoboehmite–bayerite, and if $X > 12.55$, bayerite will be immediately formed.

Investigations have been performed on the transformation of aluminum hydroxycarbonate in aqueous solutions to address the mechanism of formation of crystalline aluminum hydroxides [14]. As discussed in Ref. [15], Aluminum hydroxycarbonate is actually amorphous aluminum hydroxide in which some carbonate anions substitute for surface hydroxyl anions. The findings of this investigation indicate that when a suspension of aluminum hydroxide in water is aged at pH 7 or higher, it undergoes a two-step aging process: amorphous aluminum hydroxide transforms into poorly ordered boehmite (pseudoboehmite) [16], which in turn transforms into the stable bayerite. It has also been shown that supersaturated aluminate solutions form the most-soluble phase first, become saturated with that phase, and subsequently

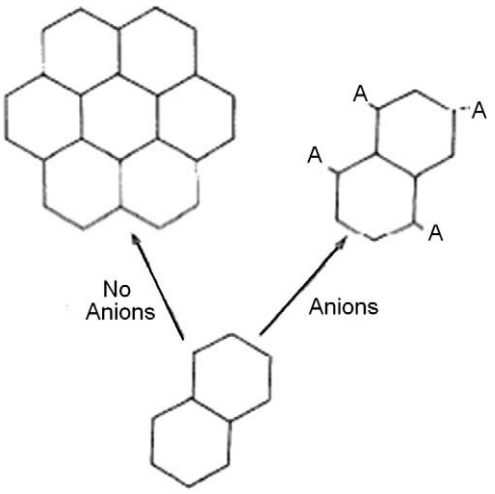

Fig. 4. Possible pathways for polymerization of $Al(OH)_3$. The A represents an anion [27].

form the next soluble phase. For example, a solution supersaturated with respect to amorphous $Al(OH)_3$, pseudoboehmite, and bayerite (phases in order of decreasing solubility) will first form the amorphous $Al(OH)_3$, then pseudoboehmite, and finally bayerite. Upon aging of the precipitate, amorphous $Al(OH)_3$ will convert first to pseudoboehmite which will subsequently convert to bayerite. The amorphous solid is initially high in both water and hydroxyl anion concentration.

The rate of transformation to the more-crystalline form is controlled by the rate at which hydroxyl anions replace water in amorphous solid [13]. Boehmite is formed by solid-state interparticle and intraparticle condensation/aggregation [14], which occurs as water is removed [17]. A hydroxyl anion reacts topochemically with another hydroxyl anion in the amorphous solid, which results in a water molecule and produces the aluminum oxyhydroxide known as boehmite under neutral or alkaline conditions [10]. It has been shown that the solubility of poorly ordered boehmite determines the rate of nucleation and growth of the crystalline aluminum polymorphs [18]. Additional support for rapid precipitation and crystallization in neutral and alkaline media to produce bayerite has been provided in Ref. [19].

By using the technology of IR and XRD, the phase transformation of amorphous aluminum hydroxide as a result of aging is studied in Ref. [20] through examination of aluminum hydroxide precipitate which was produced by titrating ammonium into aluminum chloride solution to a pH 7. XRD pattern changes as function of aging time are shown in Fig. 2. The phase transition as a function of aging time is clearly shown in the figure.

Based on previous studies, Li et al. [21] drew aging pathways for both dilute and concentrated sodium aluminum solutions. For dilute aluminate solutions, the species/particles follow the pathway shown schematically in Fig. 3(A) [21]. This involves (1) Al(III)-containing species present as Keggin ions, (2) attachment/aggregation and polymerization of Keggin ions to form larger denser supramolecular coalescent cluster, (3) growth of the cluster leading to an amorphous entity, (4) the rapid growth into nuclei or pseudospinal structures, (5) continuous growth of the nuclei into a pseudoboehmite crystalline structure and (6) eventual transformation into a more stable bayerite crystal.

In contrast, for concentrated sodium aluminate solutions (the Bayer region), the species/particles growth follows the growth mode shown in Fig. 3(B) [21]: (1) aluminate ion pairs including monomers, dimers and trimers, (2) formation of loose Al(III)-containing polymeric networks, (3) densification of the network to form a cluster, (4) further densification and growth leading to the formation of a crystalline core, (5) rapid growth of the core accompanied by nuclei agglomeration and (6) formation of a gibbsite crystal surrounded by a diffuse layer.

2.3. General cation/anion effects on aluminum hydroxide phase

Adsorption of surface-active species is well known to affect the rate and mechanism of crystal growth. The crystallization process may be retarded, or the crystal habit of the precipitate may change significantly [22], and the polydispersity of the product may be controlled by adding surface-active species to the supersaturated solution. When aluminum hydroxide precipitate is prepared by precipitation from aluminum salt solution, a highly random structure is formed. Anions present during precipitation are absorbed by the aluminum hydroxide precipitation and are believed to be important in stabilizing the colloidal system. Studies have shown that the crystallization of gibbsite from amorphous aluminum can be greatly inhibited by the presence of sulfate [23], silic acid [24] and citric acid [25], while nitrate has a rather weak effect, and perchlorate has no effect at all [26]. Fig. 4 illustrates the mechanism of anion interference to crystallization [27].

It has been found that a relatively high degree of adsorption of anions occurs when aluminum hydroxide solid is precipitated at pH conditions below 9.2 that is the zero point of charge. Based on the adsorption capacity for several anions at different pH conditions, three types of anion adsorption were reported [28]: nonspecific adsorption was suggested for anions such as nitrate, chlorate, and chloride, which are loosely held in the diffuse layer and therefore adsorbed only by positively charged surfaces; specific adsorption of anions of completely dissociated acids such as sulfate and fluoride is based on chemical adsorption and involves ligand exchange with surface of water; and the third type of adsorption is the specific adsorption of incompletely dissociated acids such as phosphate and silicate.

Precipitates produced with nitrate anions show a nitrate band split in the aluminum hydroxide solid appearing at 1395 and 1350 cm^{-1}, as compared with the undisturbed 1358 cm^{-1} IR band [27]. The splitting of the nitrate band indicates that some perturbation occurs when the nitrate anion is incorporated into the aluminum hydroxide precipitate. It has been observed that the v^3 vibration splits into two new frequencies when the nitrate anion has a lowered symmetry due to the perturbation [29]. The magnitude of the split appears to increase as the dissymmetry occurs [29]. Based on previous observations, the relatively small degree of splitting observed for the nitrate anion in the aluminum hydroxide, 45 cm^{-1}, indicates an electrostatic interaction in which the nitrate anion is outside the coordination sphere of the aluminum

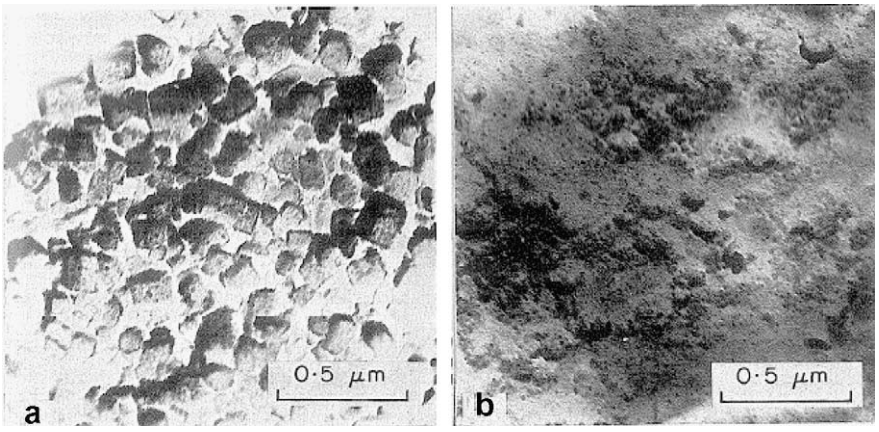

Fig. 5. Electron micrograph of the hydrolytic reaction products of Al at the initial OH/Al molar ratio of 3 and Al concentration of 1×10^{-4} M after 40 days of aging at room temperature in (a) the absence of citric acid and (b) the presence of 10^{-4} M citric acid [25].

cation, which is in good agreement with the nonspecific adsorption attributed to this anion [28].

The affinity of the carbonate anion for the aluminum cation is evidenced by the presence of carbonate in reactive aluminum precipitate [30]. Two features of the IR spectra of the carbonate containing aluminum hydroxide indicate that the carbonate anion is in a state of lower symmetry [31]. In addition, the v^3 vibration splits into two new adsorption bands at 1500 and 1435 cm^{-1} [31]. The nature of the carbonate-to-aluminum bond in aluminum hydroxide can be inferred by comparison with carbonate complexes and carbonate surface oxides [32].

Studies have also been conducted to investigate the role of organics in the crystallization of aluminum hydroxide. An example that depicts the effect of citric acid on retarding the crystallization of aluminum hydroxide is shown in Fig. 5 [25]. The noncrystalline nature of the precipitant was apparently due to the occupation of coordination sites of Al ions by citric acid, resulting in a distortion in the arrangement of the hexagonal ring units normally found in crystalline aluminum hydroxides.

Additional experiments have been conducted in which small quantities (0.50 mg) of fulvic acid (FA) were added to aluminum chloride solutions, 450 ml of a 10^{-3} M solution [7]. (FA resembles citric acid in that it contains CO_2H and aliphatic OH groups; it resembles quercetin in that it also contains phenolic hydroxyl and ketonic C=O groups. It is through these functional groups that FA can form stable complexes with Al.) The solutions were then titrated with 0.1 M NaOH to raise the pH to 6, 8, and 10. It was found that FA inhibited the formation of gibbsite at a pH 6, leading to the formation of pseudoboehmite. In the solutions with a pH 10, the addition of as little as 0.0125 mg/l of FA was sufficient to prevent the formation of any precipitate. A simple explanation may be that at pH 10 the surface of the aluminum hydroxide and FA are both negative, and then electrostatic repulsion between the two components appears responsible for the lack of precipitation.

It has been suggested that the retardation of crystallization behavior was the result of activity at the solid/solution interface [33]. Adsorption of the citrate can lead to changes of the surface charge and interfacial tension and can influence the kinetics of a number of elementary steps [31]. The principal effect, however, was suggested to be the occupation of certain surface sites, which causes the growth unit to be blocked [28]. In summary, it has been shown that the presence of certain organic agents even in small quantities is sufficient to modify the solubility of aluminum and also inhibitor crystallization.

3. Aluminum solubility in alkaline solution

3.1. Prediction of the aluminum solubility

The aluminum solubility in alkaline solution is determined by dissolution reaction of the aluminum hydroxide, whose equilibrium is a function of aluminum hydroxide phase:

$$Al(OH)_3 = Al^{3+} + 3OH^-, \tag{4}$$

with the thermodynamic solubility product (K_{sp}) as

$$K_{sp} = [Al^{3+}][OH^-]^3, \tag{5}$$

where [ ] represents the species concentration. So the concentration of aluminum can be obtained:

$$[Al^{3+}] = K_{sp}[H^+]^3/K_w, \tag{6}$$

where K_w is the equilibrium constant. In alkaline or acidic solution, aluminum can exist as the following forms: Al^{3+}, $Al(OH)_4^-$, $AlOH^{2+}$, $Al(OH)_2^+$, $Al(OH)_3^0$. So the total solubility of the aluminum in the solution can be expressed by

$$\sum Al(aq) = [Al^{3+}] + [Al(OH)^{2+}] + [Al(OH)_2^{3+}] + [Al(OH)_3^0] + [Al(OH)_4^-]. \tag{7}$$

Concentration of each Al–OH complex can be related to that of Al^{3+} through the following cumulative complexation reactions [34]:

$$Al^{3+} + H_2O = AlOH^{2+} + H^+, \tag{8}$$

$$Al^{3+} + 2H_2O = Al(OH)_2^+ + 2H^+, \tag{9}$$

$$Al^{3+} + 3H_2O = Al(OH)_3^0 + 3H^+, \tag{10}$$

$$Al^{3+} + 4H_2O = Al(OH)_4^- + 4H^+. \tag{11}$$

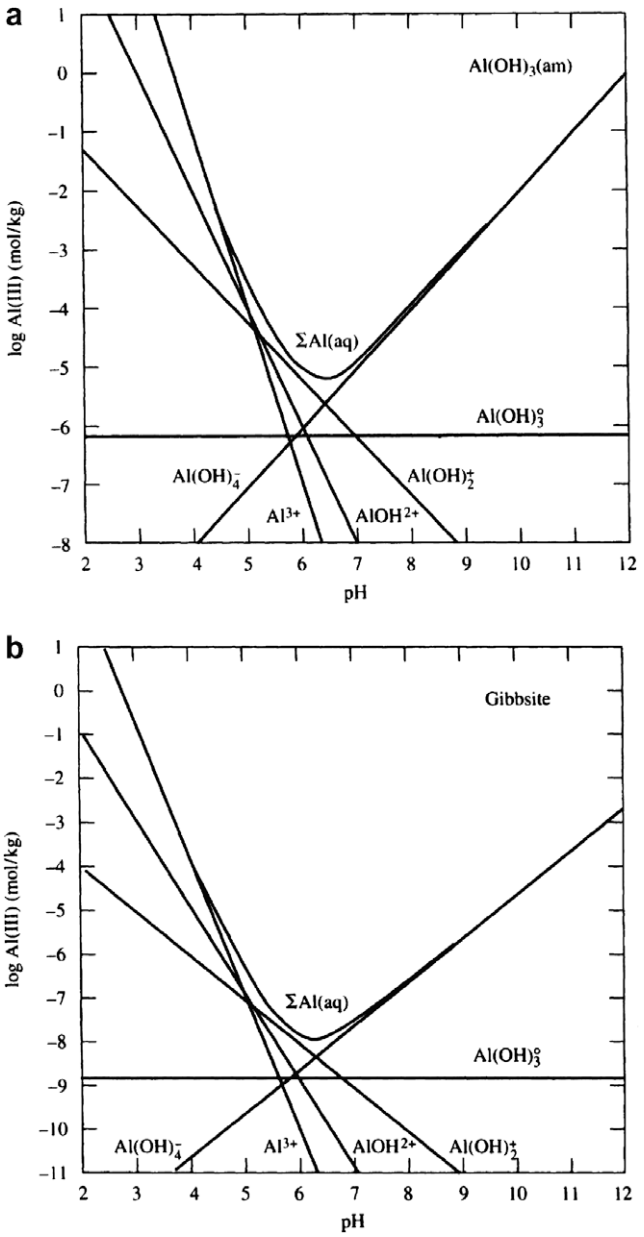

Fig. 6. Solubility of (a) amorphous $Al(OH)_3$, and (b) gibbsite [$Al(OH)_3$], as a function of pH at 25 °C. Also shown are lines indicating the solubility concentrations of Al^{3+} and individual hydroxyl complexes [34].

The complexation constant expressions for these reactions are

$$K_8 = \frac{[AlOH^{2+}][H^+]}{[Al^{3+}]}, \quad K_9 = \frac{[Al(OH)_2^+][H^+]^2}{[Al^{3+}]},$$
$$K_{10} = \frac{[Al(OH)_3^0][H^+]^3}{[Al^{3+}]}, \quad K_{11} = \frac{[Al(OH)_4^-][H^+]^4}{[Al^{3+}]}.$$

Then Eq. (7) can be rewritten as

$$\sum Al(aq) = \frac{K_{sp}}{K_w^3}([H^+]^3 + K_8[H^+]^2 + K_9[H^+] + K_{10} + K_{11}/[H^+]). \quad (12)$$

The equilibrium data for the above reactions can be found in Ref. [8]. For an example, at 25 °C, $K_8 = 10^{-5.00}$, $K_9 = 10^{-10.1}$, $K_{10} = 10^{-16.9}$, $K_{10} = 10^{-22.7}$ and $K_{sp} = 10^{-31.2}$ for amorphous aluminum hydroxide and $10^{-33.9}$ for gibbsite. The equilibrium solubility of different forms and the corresponding total aluminum concentration in the solution are shown in Fig. 6 [34]. The figure indicates that the main form is $Al(OH)_4^-$ in alkaline solution, while the aluminum ions are not stable. A comparison of Fig. 6(a) and (b) indicates that the amorphous aluminum yields soluble concentrations that are significantly larger than the concentrations for the crystalline gibbsite. The total aluminum concentration reaches its smallest value near the neutral point, and it increases with increasing pH in alkaline solution and decreases with increasing pH in acidic solution. The figure can be used to predict the aluminum concentration in solution at temperature 25 °C, while the solubility at other temperatures can be obtained by using Van't Hoff relations. Conformation that the aluminate ion is the only significant species in alkaline hydroxide solutions containing less than about 1.5 M total aluminum up to temperatures of 100 °C has been provided via Raman and NMR studies [8]. Experimental results have shown that the polynuclear Al complexes play no role unless the Al concentration is moderately high (>.1 M) [35].

3.2. Effects of organic complex agents on aluminum solubility

It has been noted that organics can increase the aluminum solubility in alkaline solution as described in Ref. [36]. Speciation calculations for typical hydroxyl organic ligands and their aluminum complexes can be performed based on established protonation constants and reaction quotients [37]. Citric acid has been investigated and found to establish three aluminum complexes: the 1:1 complex, its protonated and deprotonated forms.

Experimental evidence for the effectiveness of chelating agents has been found [7]. Catechol has been observed to have the highest stability. Ethylenediaminetetraacetic (EDTA) is another polydentate complexing agent that forms complexes with many metals. The anion of EDTA has a quadruple negative charge. The four carboxylate ion groups and also the two nitrogen atoms can form bonds with aluminum. Another promising chelating agent is desferriferrioxamine (Desferal R DFB). This agent is a microbial siderophore that has been used for the treatment of Colley's anaemia and is now being used for the treatment of aluminum overload [11].

Polybasic acids have also been studied in conjunction with altering the solubility of aluminum hydroxide [11]. In this study 20 ml of 0.1 M $AlCl_3$ was titrated with 0.1 NaOH. Prior to titration an appropriate quantity of potassium acetate, oxalate, or citrate was dissolved in $AlCl_3$ solution. It was found that increasing amounts of the organic acid delay the onset of precipitation and, in the case of citric acid, precluded precipitation if a molar ratio of citric acid to aluminum is above 0.475. An infrared analysis of the air-dried 1:1 citrate to aluminum complex indicated that the complex may be similar to commercial aluminum citrate [11]. From these studies it appears that the strength of the aluminum–anion bound is in the order: citrate > oxalate > acetate.

As a result of formation of organic complexes, the dynamics of nucleation are significantly affected by adding organics into the solution. In investigations using aluminum chloride with citric acid, using quasi-elastic light scattering, it has been found that the addition of citric acid changed the dynamics of both solutions and suspensions [38]. In solutions of very high hydrolysis (OH/Al = 3.29), particles did not form when the mole/mole ratio of citrate to aluminum equaled 0.8. Under the same hydrolysis conditions but at citrate/Al ratios less than 0.8, particles formed, and nucleation and growth were markedly slowed. Under conditions of high hydrolysis (OH/Al = 2.46), particles also formed in the presence of citric acid when base was added, but the rate of formation was slowed.

4. Aluminum–boron complex

4.1. Boron behavior in the solution

In a pressurized-water-reactor (PWR), boric acid is present in the reactor core to balance the pH of the primary coolant. During a LOCA, the coolant with a pH of approximately 10 is injected into the emergency-core-cooling-system (ECCS). The interactions between the boron and the aluminum corrosion products can result in precipitates that affect the efficiency of ECCS. Therefore, the boron–aluminum interactions are of paramount importance during post-LOCA in a PWR containment environment. Considering that boron is an essential element for plant growth, boron adsorption on solid surfaces is of interest in soil solution because it plays a pivotal role in determining the amount of boron available for plant uptake.

Boric acid is a Lewis acid, hydroxyl acceptor, and through hydrolysis produces a change in coordination from planar to tetrahedral [35]. The dissociation constant for boric acid pK = 9.24, and therefore boric acid exists predominantly as un-dissociated boric acid $[B(OH)_3]$ in dilute aqueous solution below pH 7. Above pH 10, the metaborate anion $B(OH)_4^-$ becomes the main species in solution. Between pH 6 and pH 11 and at high concentration (>0.025 M), highly water soluble polyborate ions such as $B_3O_3(OH)_4^-$, $B_4O_5(OH)_4^{2-}$, and $B_5O_6(OH)_4^-$ may be formed [35].

Calculation of the aqueous solution chemistry of boron is generally confined to hydrolysis due to the lack of thermodynamic data for aqueous cation complexes containing boron. However, there has been one investigation which reports thermodynamic data for the aluminum boron complex [39]. These data have drawn critical comments from several sources [40]. Furthermore, the kinetic data have been unsuccessful in explaining the appearance of a white amorphous precipitate that appeared in a test consisting of [Al] = 0.005 and [B] = 0.04 M solution titrated with sodium hydroxide [41], furthermore it is difficult to detect the chemical complexes based on ^{27}Al and ^{11}B NMR measurements at either pH 2 or pH 12.

Previous investigations revealed that aluminum borate complexes are present at 25 °C using ^{27}Al NMR via measurements of gibbsite and boehmite solubility in the presence of boric acid [42]. The ^{27}Al spectra performed at pH 9 in Al–B solutions with [B] = 0.02 M shows the presence of two peaks at 80.5 and 74.5 ppm, which correspond to $Al(OH)_4^-$ and a single substituted dimmer, $Al(OH)_3OB(OH)_2$. In 0.08 and 0.2 M borate solution, a third peak appears at 68.5 ppm, which can be assigned to $Al(OH)_2O_2(B(OH)_2)_2^-$. Solubility studies were also performed that allow for the determination of the equilibrium constant for the dimmer reaction:

$$Al(OH)_4^- + B(OH)_{3aq}^0 = Al(OH)_3OB(OH)_2^- + H_2O. \quad (13)$$

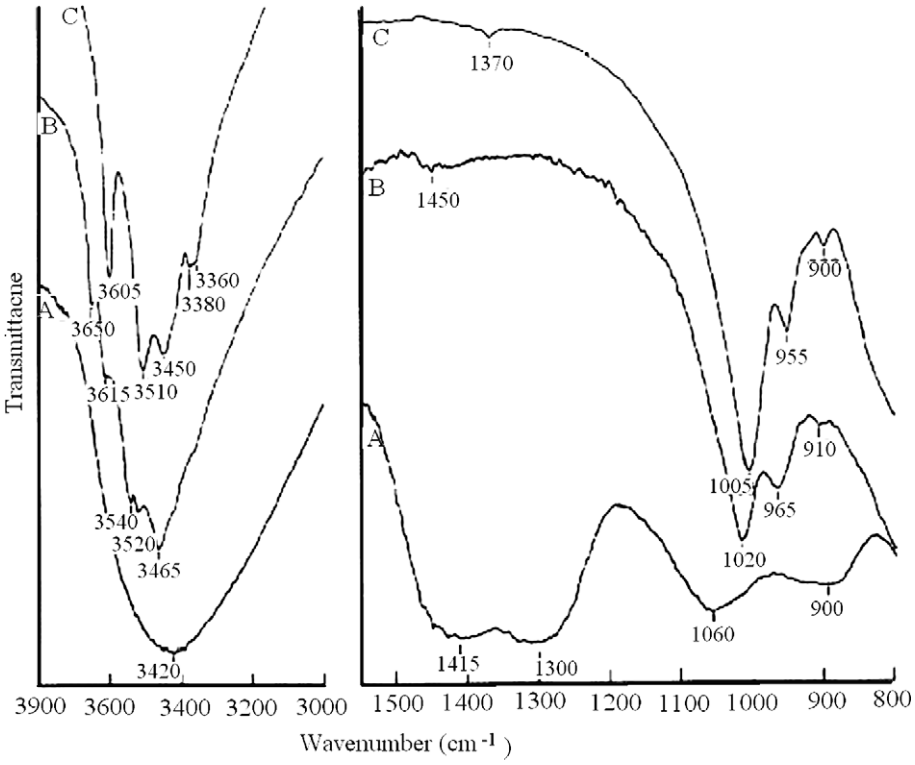

Fig. 7. Spectra of (A) $Al(OH)_3$ with boron (89 days old), (B) $Al(OH)_3$ prepared without boron (13 days old), and (C) commercially prepared $Al(OH)_3$ [27].

The equilibrium constant has been found to be

$$\log K = (241.94 \pm 130.7)/T + (0.81 \pm 0.36). \quad (14)$$

The impact of the aluminum borate complex on the equilibrium has been shown to result in a significant increase in aluminum solubility (up to factors of 6) for both gibbsite and boehmite [39].

Finally, it should be noted that aluminum borates have been synthesized by a precipitation process in which dilute solutions of aluminum nitrate nonahydrate $Al(NO_3)_3{:}9H_2O$ and boric acid are precipitated into a basic solution of ammonium carbonate. It was found that until excessive heating was applied, the material was largely amorphous in nature [43–45].

4.2. Boron adsorption

Adsorption of boron may be explained by various mechanisms, including ligand exchange, formation of bidentate surface complexes, and incorporation into lattices. Ligand exchange is reversible with respect to pH changes, however, anion desorption at constant pH exhibits varying degrees of irreversibility [46]. In a study of the adsorption of boron onto aluminum hydroxide surfaces, a solution was synthesized by the drop-wise addition ($\sim$2 ml min^{-1}) of 0.5 M NaOH (the base typically contained 0.75 M H_3BO_3) into 100 ml of 0.5 M $AlCl_3$ until the pH was 7.0. The solution was then analyzed using IR analysis [23] and the boron content, with respect to the $Al(OH)_3$, was then determined. It was found that the boron present in the hydroxide solid is held predominantly on the hydroxide surface as a specifically absorbed ion. This mechanism of anion exchange with hydroxyl ions leads to specific surface adsorption [27] which produces a shift in the zero point of charge of the mineral to a more-acid value.

Previous studies indicate that the adsorption of boron onto the aluminum surface precludes crystallization. Fig. 7 presents the IR results obtained as a result of aging the aluminum hydroxide precipitates [27]. As may be seen, the commercially prepared hydroxide shows three well-resolved peaks in the OH stretching region at 3605 cm^{-1}, 3510 cm^{-1}, and 3450 cm^{-1} and a doublet at 3380 cm^{-1} and 3360 cm^{-1}. These bands are characteristic of gibbsite. The 13-day aged solution without boron also shows evidence of a high degree of structural order. These peaks indicate a gibbsite and bayerite mixture. In contrast, the aged boron-containing hydroxide exhibits a very broad adsorption band in the OH stretching region, centering at 3420 cm^{-1}. The absence of any sharp peak confirms the hypothesis that boron is held directly on the hydroxide surface, thereby inhibiting the polymerization process.

Identification of the boron absorbed onto the amorphous aluminum was obtained by examining the IR spectra in the 800–1500 cm^{-1} region as shown in Fig. 7. While the 1020 cm^{-1} and 965 cm^{-1} adsorption bands are not present in the precipitate with boron, two broader peaks appear at 1060 cm^{-1} and 900 cm^{-1}. In

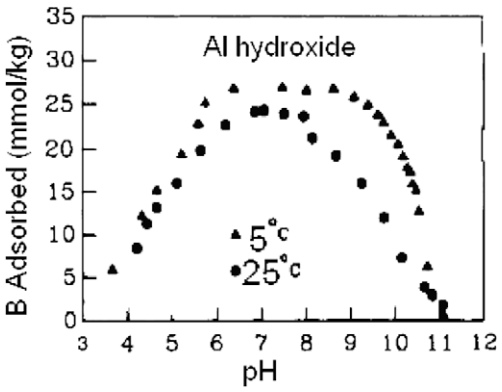

Fig. 8. Absorbed boron as a function of pH at 25 °C and 5 °C [48].

addition, two new bands have also appeared at approximately 1415 cm^{-1} and 1300 cm^{-1} [27].

Another means by which to evaluate the adsorption of an ion is the change in the zero point of charge (ZPC). ZPC defined as the pH at which the net surface charge is zero or the minus anion exchange capacity equals zero. Specific adsorption of an anion makes the surface to which it is adsorbing more negatively charged. This specific adsorption produces a shift in the ZPC to a more-acidic value. Specifically adsorbed ions are held in inner-sphere surface complexes that contain no water between the adsorbing in and the surface functional group. Kinetic experiments using pressure-jump-relaxation have also been used to confirm that boron adsorption proceeds as an inner-sphere complex on aluminum oxide via a ligand exchange of borate with surface hydroxyl groups [47]. The ZPC for the $Al(OH)_3$ free of any specifically adsorbed anions is 9.72, whereas for the boron-containing gel, the ZPC was found to be 7.57–8.14 [27].

In another study on the adsorption of boron onto amorphous aluminum, attenuated total reflectance Fourier transform infrared spectroscopy (ATR-FTIR) was utilized [48]. The study of aqueous solutions of metal ligand systems by conventional IR spectroscopy is limited because water absorbs energy in several areas of the IR spectrum, resulting in very strong, broad bands in the regions 3650–2930, 1720–1580 and 930–400 cm^{-1}. To minimize this, it is necessary to use solutions of high concentrations in cells with very short optical path lengths, resulting in a poor band resolution. ATR-FTIR overcomes these problems and allows an IR spectrum of an aqueous solution of a metal ligand to be observed [49]. It was found that trigonal B asymmetric bands shifted to higher frequencies and indicated that both $B(OH)_3$ and $B(OH)_4^-$ are absorbed via a ligand exchange mechanism [48].

Measurement of boron adsorption was carried out [48] through measuring the boron concentration using a technicon autoanalyzer and the azomethine method [50]. The total boron adsorbed was the difference between the total boron added and the boron remaining in solution. Results of this study are shown in Fig. 8. As may be seen in this figure, decreasing temperature favors absorption. This is mainly because increasing temperature decreases the ZPC. A decrease in ZPC renders the surface more negative at a given pH and, therefore, decreases the adsorption of anions. It should also be mentioned that adsorption is maximized onto high-surface-area materials. The adsorption results at low temperature are also consistent with the ^{27}Al measurements which indicate complexation between aluminum and boron is favored at low temperature.

Additional insight into the nature of the aluminum–boron surface complex coordination was obtained using ATR-FTIR [48]. It was found that the broad bands at 1410 and 1148 cm^{-1} are assigned to the B–O asymmetric stretching of triagonal boron and to B–OH in plane bending of trigonal boron. These bands are seen to increase in intensity with increasing boron concentration. At pH 9, which is near the pKa for the monomeric boron species, roughly half of the total boron is in the form of $B(OH)_3$, and half is in the form of the $B(OH)_4^-$ anion. The band at 955 cm^{-1} is assigned to the asymmetric stretching of tetrahedral boron, and the broad band at 1154 cm^{-1} is a mixture of B–OH bending of both triagonal and tetrahedral boron. Based on the above data, the most useful diagnostic bands are at 1410 cm^{-1} for asymmetric stretching of triagonal boron and at 955 cm^{-1} for asymmetric stretching of tetrahedral boron.

At higher pH, the B–O asymmetric stretching of triagonal boron is not significantly shifted compared with 1410 cm^{-1}, pure boric acid. However, the B–OH bending of the triagonal boron band resulted in a narrower width and a higher wave number of 1266 cm^{-1} from 1148 cm^{-1} due to the complexation on the amorphous aluminum [48].

Attempts to characterize the tetrahedral boron failed due to severe band interference in the range of 1000–900 cm^{-1} from the Al–O bond, which has a strong absorbance at 969 cm^{-1}. Although, the tetrahedral boron is the dominant species at pH 10.2 in aqueous solution, it need not be the dominant absorbed species on amorphous aluminum due to the negative charge on the solid surface at this pH. The appearance of the triagonal boron on the surface of the amorphous aluminum at pH 10.2 suggests that the neutral $B(OH)_3$ species could be preferred due to its higher affinity for the negatively charged surface of the amorphous aluminum than for the borate ion, which would experience charge repulsion.

Several surface complexation models are available to describe the adsorption of boron onto aluminum surfaces. These chemical models provide a molecular description of adsorption using an equilibrium approach with mass action and mass balance equations. In these models, boron adsorption occurs via complex formation with surface hydroxyl groups on aluminum. Surface complexation models define surface species, chemical reactions, mass balance, and charge balances and calculate thermodynamic properties such as activity coefficients and equilibrium constants. Two models that are particularly well suited for studying boron's adsorption onto amorphous aluminum surfaces are the constant capacitance model and the triple-layer model.

The constant capacitance model of the oxide aqueous solution interface has been applied to describe boron adsorption on aluminum [51]. In the constant capacitance model, anion adsorption is assumed to occur via a ligand exchange mechanism with the reactive surface functional group, AlOH; no surface complexes are formed with ions in the background electrolyte. Specifically adsorbed ions reside in the surface plane of adsorption along with protons and hydroxyl ions. (In some cases, chemically unrealistic values of the protonation–dissociation constants were obtained, potentially reducing the chemical significance of the model application [52].)

The triple-layer model has also been applied to describe boron adsorption on aluminum [52]. In contrast with the constant capacitance model, the triple-layer model allows for anion adsorption to occur specifically via ligand exchange or nonspecifically through the formation of outer-sphere surface complexes with the reactive surface functional group, AlOH. Outer-sphere complexes contain at least one water molecule between the adsorbing ion and the surface functional group. The triple-layer model always includes outer-sphere complexation reactions for ions of the background electrolyte. Surface reactions, equilibrium constants, mass balance,

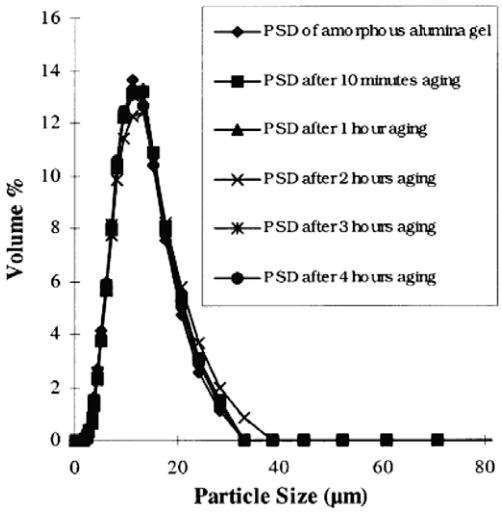

Fig. 9. Particle size for aluminum in pH 11.0 solution [56].

and charge balances for the application of the triple-layer model are provided in Goldberg 1993 [53]. It has been found however that only the inner-sphere adsorption mechanism could successfully describe both equilibrium and pressure jump kinetic data using the triple-layer model [47].

5. Particle size distribution

The aluminum behaviors such as the solubility in alkaline solution are functions of the particle size distribution that is affected by the aluminum hydroxide phase and the organic elements.

Previous investigations into the particle size distribution of aluminum have been made using dynamic light scatting (DLS), Small-angle X-ray scattering (SAXS), and acoustic techniques [6,54,55]. A typical particle size distribution at pH 11 for different aging time is shown in Fig. 9 [56]. Clearly, the volume-based distribution remained unchanged with aging time for the case considered, indicating that the particles are very stable against aggregation. This phenomenon is due to the fact that the particles repel one another because of the balance of the repulsive and attractive forces that exit between particles as they approach on another. If all the particles have a mutual repulsion, the dispersion will remain stable. However, if the particles have little or no repulsive force, some instability mechanism will eventually take place, e.g., flocculation, aggregation, etc.

The degree of particle repulsion can be measured using a zeta potential. The zeta potential of a particle is the overall charge that the particle acquires in a particular medium. The magnitude of the measured zeta potential is an indication of the repulsive force that is present and can be used to predict the long-term stability of the product. If all the particles in suspension have a large negative or positive zeta potential, they will tend to repel each other, and there is no tendency for the particles to come together. However, if the particles have low zeta potential values, there is no force to prevent them from coming together and flocculating. As the pH is raised by adding base, such as NaOH, the electrical barrier is lowered from a large positive value to zero at around 9.0 and then to a negative potential at high pH, i.e., >9, the system is again stable against further aggregation as shown in Fig. 9.

The particle size distribution is also a function of the aluminum concentration in the solution. By using SAXS [55], Bale and Rausch measured the particle size in nitrate and chloride solutions with changing aluminum concentration. When the aluminum concentrations is 0.25 M Al, the average radius and thickness of the particles were determined to be 88 nm and 5 nm, respectively, with pH between 7 and 9.8. At reduced concentrations of 0.005 M Al, the radius and thickness of the particles were found to be approximately 20 nm and 4 nm, respectively. The 'platelet' shape that was assumed in the analysis has indeed been found to be representative of aged, dried gels, and gibbsite, as well as boehmite, has a tendency to form platelets.

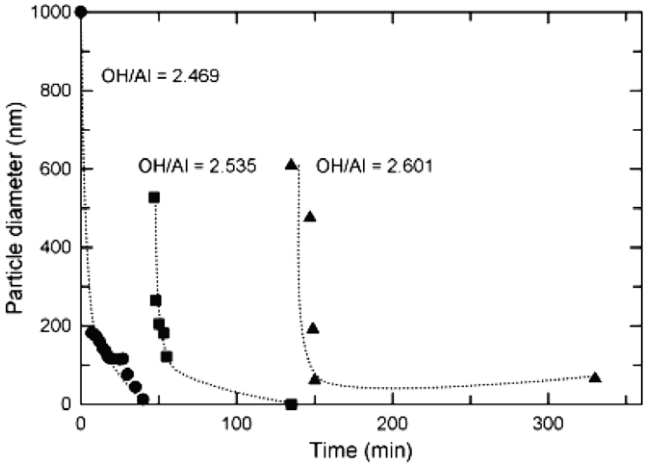

Fig. 10. Particle growth dynamics in aluminum chloride solutions as a function of time for various OH/Al ratios at ambient temperature [38].

Dynamic studies of the particle size have also been conducted using quasi-elastic light scattering [38]. In these investigations, it was found that in solutions of aluminum chloride, large particles that were quickly formed subsequently shrank until sufficient hydroxide was added, as shown in Fig. 10.

6. Aluminum corrosion

6.1. Corrosion mechanism

It is well known that aluminum metal is very inert in neutralized solution, while pure aluminum is too reactive to be used in concentrated alkaline solutions [57]. Experimental results show that there are two competing processes at the aluminum metal surface: direct dissolution of the aluminum metal and electrochemical formation/dissolution of the aluminum hydroxide films. The first process is very intense, which leads to a high corrosion rate. With elapsed time a film forms on the metal surface which acts as a barrier for species transport. Therefore, the corrosion rate is significantly reduced after the film forms.

Taking into account that $Al(OH)_4^-$ is the only stable form of aluminum in alkaline solution as shown in Fig. 6, the direct dissolution of aluminum is due to the following reaction:

$$Al + 3H_2O + OH^- = \frac{3}{2}H_2 + Al(OH)_4^-. \quad (15)$$

Clearly, the direct aluminum dissolution is accompanied by hydrogen production. Gas bubbles have been observed at the aluminum metal surface experimentally. Therefore, the corrosion of pure aluminum in alkaline solution proceeds mainly by water reduction according to Eq. (15). The reaction [Eq. (15)] indicates that the dissolution rate depends on the concentrations of OH^- and aluminate ions $Al(OH)_4^-$ at the solid/liquid interface. So the transportation of OH^- and $Al(OH)_4^-$ in the solution to and from the interface, respectively, is expected to play important roles on the aluminum dissolution rate [57]. If the reaction at the interface is much faster than the transport into the solution, the dissolution rate is determined by the transport rate. In this later case, the aluminum corrosion rate will increase as the transport affinity is increased. This increased transport propensity will increase by increasing solution velocity. However, if the transport rate is greater than the reaction rate, the aluminum corrosion rate is determined by the reaction rate and depends little on the transport of OH^- and $Al(OH)_4^-$ through the solution, which has been reported by several researchers such as Refs. [58,59].

The electrochemical formation of hydroxide film on pure aluminum surface in alkaline solution has been verified experimentally via an open circuit [60]. And it is also considered by several other authors such as Refs. [57,60–64]. The potential changes at aluminum surface in alkaline solution as a function of time are shown in Fig. 11 [64]. The potential increases with time elapsing until it reaches a constant value. The increase in potential with time is known to arise from the growth of a surface oxide film [65].

As discussed in Ref. [57], the film formation is due to the following reaction:

$$Al + 3OH^- = Al(OH)_3 + 3e^-. \quad (16)$$

The film forms due to the inwards diffusion of OH^- through the film. When a film with considerable thickness forms, the direct dis-

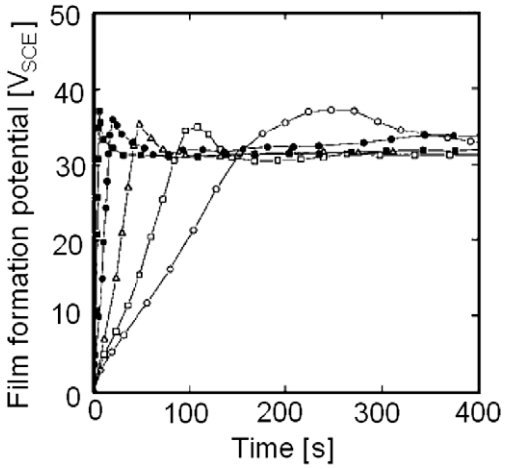

Fig. 11. Changes in film formation potential obtained from the pure aluminum rod specimen with time in 10–3 M NaOH solution at various applied anodic current densities of: ○, 5 mA cm^{-2}; □, 10 mA cm^{-2}; △, 20 mA cm^{-2}; ●, 50 mA cm^{-2}; □, 100 mA cm^{-2} [64].

solution of aluminum metal ceases as well as the hydrogen production. After that, the aluminum corrosion can be classified into a direct metal dissolution by the movement of aluminum ions through the film and an indirect metal dissolution by consecutive oxide film formation and dissolution [57]. Because Al^{3+} is not thermodynamically stable in alkaline solution, the direct ejection of aluminum ions from the film into the solution can never occur, which was shown in Refs. [64, 66]. So the aluminum corrosion after the film formation is due to the following reaction:

$$Al(OH)_3 + OH^- = Al(OH)_4^-, \quad (17)$$

Therefore, the corrosion of pure aluminum in alkaline solution can be divided into two sub-steps of a partial anodic reaction comprising the electrochemical formation and chemical dissolution reactions of the film, and partial cathodic reaction of water reduction reaction [57].

In some applications, oxide layers are pre-formed on aluminum metal surfaces to protect the substrate. The oxide layer composed of Al_2O_3 is compact and protective in neutral solution. However, the film can be attached by OH^- in alkaline solutions, resulting in film dissolution. If the oxide films were completely uniform, both physically and chemically, it would be expected that the thinning would be uniform over the whole surface. If not, it would be expected that the normal dissolution process would be a flaw-assisted process or a flaw-centered process which has been well demonstrated in series of experiments [4]. The dissolution of the oxide film is due to the following reaction:

$$Al_2O_3 + 2OH^- + 3H_2O = 2Al(OH)_4^-. \quad (18)$$

It should be noted that the dissolution of the aluminum oxide is much slower than the direct dissolution of aluminum metal [Eq. (15)]. On the other hand, the aluminum oxide can be converted into aluminum hydroxide if OH^- ions take up the vacancies left by oxygen inwards diffusion according to the following reaction:

$$Al_{Al}(ox) + \frac{3}{2}V_O^{2+} + 3OH^- = Al(OH)_3. \quad (19)$$

Therefore, with time elapsing, the oxide layer may be covered into a hydroxide layer.

6.2. Corrosion rate

The corrosion rate of aluminum in alkaline solution is a function of the operating conditions such as the temperature, the pH, the solution properties, etc. More specifically, the corrosion rate depends on the time in a static solution. Because the aluminum concentration in the solution increases, the average corrosion rate decreases with time elapsing. Therefore some different authors report very different corrosion rates of aluminum in alkaline solution because of the different exposure time. In this subsection, we will review experimental data on aluminum corrosion in alkaline solution.

It has been experimentally found that the corrosion rate depends logarithmically on the pH [62], different dependencies being noted on either side of the pH at which the corrosion rate is at its minimum (close to pH 6). These results were reported by Chatalov [67] and Pourbaix et al. [68]. Vujicic and Loverecek [69] obtained a different logarithmic relation between the corrosion rate and pH value. The curves of corrosion rate as a function of pH from Ref. [69] are shown in Fig. 12. Clearly, for systems considered in the reference, the point of minimum corrosion rate is above pH 7.0 which is greater than the pH value obtained by Chatalov [67]. On the other hand, Vujicic and Loverecek reported corrosion rates about 50% higher than those of Chatalov's. Long-term corrosion test results of aluminum in sodium hydroxide solution over the pH range of 8–13 were carried out by McKee and Brown [70] up to one week and over the pH range of 7–12 were carried out by Tabrizi et al. [62] up to 80 days. A summary of corrosion rate data of aluminum in alkaline solution are given in Table 3.

Table 3 indicates that the corrosion rate depends on the exposure time, which is clearly shown in Fig. 13. Over 40 days immersion, the weight loss increased with time elapsing. For immersion times beyond 40 days, in solution of pH 10 and 11, the weight losses were similar to these measured at 40 days, indicating that there is no significant weight loss during the last 20 days. Generally similar trends were evident for immersion at 60 °C [62], with initial high rates of weight loss which decreased with immersion time, particularly beyond 20 days. The weight losses are converted into corrosion rates which were shown in Fig. 14. Clearly, the corrosion rate of aluminum in alkaline solution depends strongly on the exposure time. It decreases with the increasing exposure time. The dependence on exposure time is due to the increasing aluminate concentration with time whose rate is determined by the ratio of the sample surface to the solution volume. Therefore, when we

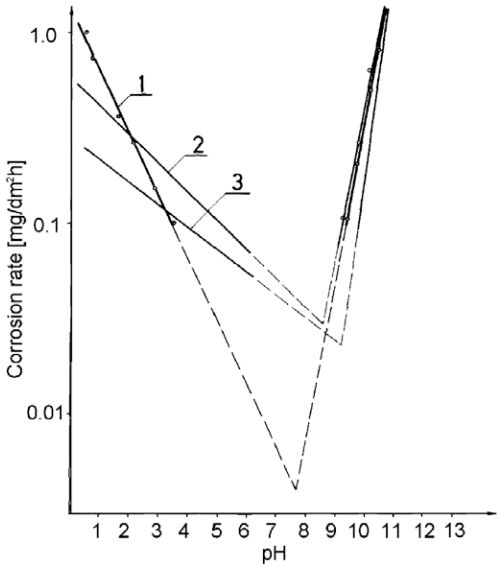

Fig. 12. Corrosion rate as function of pH in systems 1: Aluminum in 10^{-4} M KCl; 2: Aluminum in 10^{-4} M KCl containing 10^{-4} M ethylenediamine; 3: Aluminum in 10^{-4} M KCl containing 10^{-4} M ethylenediamine [69].

Table 3
Corrosion rate of aluminum in static alkaline solution.

pH	Temperature (°C)	Corrosion rate ($g^{-2}y^{-1}$)	Exposure time	Comments
9	25	22	Short term	Ref. [67]
	25	45	1 h	Ref. [69]
	25	<30	7 days	Ref. [70]
	60	242	7days	Ref alloy
10	25	280	Short term	Ref. [67]
	25	355	1 h	Ref. [69]
	25	55	7 days	Ref. [70]
	30	110	40 days	Ref. [62], solution replenished
	30	130	40 days	Ref. [62], 1000 wppm Cl^-
	60	165	40 days	Ref. [62], solution replenished
	60	65	40 days	Ref. [62], 1000 wppm Cl^-
11	30	270	40 days	Ref. [62], solution replenished
	30	285	40 days	Ref. [62], 1000 wppm Cl^-
	60	590	40 days	Ref. [62], solution replenished
	60	170	40 days	Ref. [62], 1000 wppm Cl^-

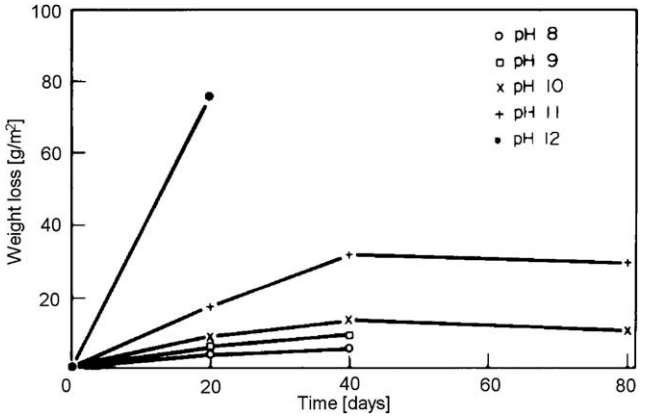

Fig. 13. The variation of weight loss of aluminum with exposure time at 30 °C [62].

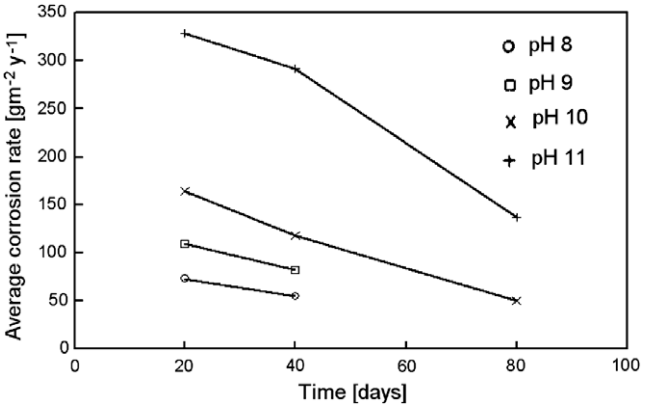

Fig. 14. Corrosion rates based on weight loss in Fig. 13.

refer to the corrosion rate of aluminum, one must consider the surface/volume ratio and the exposure time. This dependence may also explain why different authors obtained different corrosion rates in analogous systems.

Because the reaction and diffusion rates increases with temperature increasing, the corrosion rate of aluminum in alkaline solution becomes larger as the temperature increases as shown in Table 3. By plotting the corrosion current in 5 M KOH solution as a function of temperature, Chu and Savinell [58] obtained an estimate of the activation energy $\Delta G \approx 13.7$ kcal/mol for the corrosion of aluminum in alkaline solution which agreed very well with the value 12.3 kcal/mol reported in Ref. [71]. Chu and Savinell also reported that the film formed on metal surface becomes thinner with increasing temperature, allowing OH^- to more readily diffuse through the film, thus increasing the rate of aluminum dissolution.

As discussed in Section 3.2, adding organic or inorganic ions into the solution has a significant effect on the aluminum concentration. As a result, these ions affect the corrosion rate. For example, the addition of 1000 wppm Cl^- reduces the rate by two-thirds of that experienced in chloride-free solution as shown in Table 3 at 60 °C and pH 10. The ions' effects depend on the temperature. As indicated in the table, the addition of 1000 wppm Cl^- has little effect on the corrosion rate at 30 °C.

The corrosion rate may also be changed by changing the composition of the aluminum metal through adding small amount of other elements, such as Zn, Bi, Te, In, Ga, Pb, and Ti. Corrosion rates of various aluminum alloys were conducted by Macdonald et al. [72] and the results are shown in Table 4. The table indicates that the binary alloys containing <1% of the alloy elements, exhibit corrosion rates in 4 M KOH at 50 °C that are higher than that for pure aluminum. Addition of two or more alloying elements can result in a sharp reduction in the corrosion rate to well below that for aluminum. Several alloys containing Ga, In, Te, and P appear to significantly reduce corrosion. The corrosion rate of Al–0.1%In alloy was also considered by Wilhelmsen et al. [73]. It was reported in Ref. [73] that Al–0.1%In has excellent corrosion resistant properties, which is contradicts the results of Ref. [72].

In a static solution, the corrosion rate is a function of exposure time. With time elapsing, the corrosion can stop eventually when corrosion product reaches its equilibrium concentration or solubility. This is not true for a flowing system. The flow can take the corrosion product away from the metal and also can bring the reactants to the metal surface that accelerates the dissolving process. The dependence of corrosion rate on the flow velocity can be simply expressed as shown in Fig. 15 [74]. The figure indicates that at low velocities, the corrosion is controlled or partially controlled by mass transfer, in other words, the dissolution rate is greater than the mass transfer rate and the corrosion product interface concentration is at saturation or equilibrium. In such cases, the thickness of the laminar mass transfer layer becomes thinner with increasing velocity and as a result, the corrosion rate increases; when the velocity exceeds a critical value, the mass transfer rate becomes high enough to take all the corrosion products away for the interface. At this point the corrosion rate is determined by the dissolution/reaction rate and independent on the flow velocity and the corrosion now is activation controlled. For very high veloc-

Table 4
Corrosion rate on various aluminum alloy in 4 KOH at 50 °C [72].

Element	Composition (wt%)	Corrosion rate (mg/cm^2/min)
Pure Al	99.99	0.515
	99.999	0.876
	Alcoa1100-H14	2.735
Zn	0.1	1.030
	0.5	1.074
	1.0	1.097
	5.0	1.190
Bi	0.1	0.593
	0.5	0.461
	1.0	0.520
	5.0	0.507
Te	0.01	0.525
	0.05	0.584
	0.1	0.523
	0.5	0.529
In	0.01	1.910
	0.05	2.287
	0.1	1.965
	0.5	2.106
Ga	0.01	8.740
	0.05	5.707
	0.1	5.845
	0.5	7.627
Pb	0.5	0.736
P	0.2	0.918
	0.5	0.846
0.1%P, 0.1%Ga		153.351
0.1%P, 0.1%In, 0.2%Ga, 0.01%Ti		0.057
0.07%In, 0.2%Ga, 0.01%Ti		0.051
0.05%In, 0.01%Ti		0.980
0.05%In, 0.05%Ti		0.733
0.2%In, 0.05%Ti		0.621
0.25%In, 0.01%Ga, 0.1%Ti		0.041
0.1%In, 0.2%Ga, 0.1%Ti		0.048

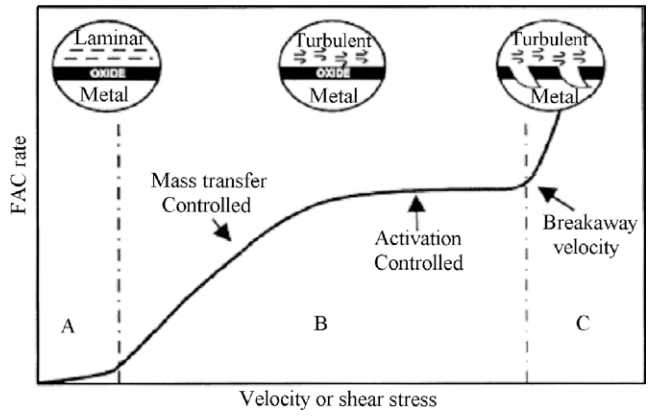

Fig. 15. Dependence of corrosion rate on the flow velocity, FAC rate = flow accelerate corrosion rate [74].

ities, the high shear stress at the interface can strip the protective film on the surface of the structure. Some cavities appear at the interface and corrosion rate increases sharply with the flow velocity. Therefore the dependence of corrosion rate of aluminum in a dynamic driven alkaline solution is a function the flow velocity. In different flow velocity ranges, the dependence may be much different. This conclusion can explain why several authors [58,59] reported that the transport of OH^- and $Al(OH)_4^-$ has little effect on the corrosion rate, while others [1] found the corrosion rate increasing with the flow velocity increasing. Unlike the static solution, the corrosion rate is a constant in a flowing system when the flow is at a steady state.

Table 5
Effect of some organic and inorganic additives on the corrosion of Al in NaOH solutions.

[NaOH]	Additive	[Additive]	Efficiency (%)
5 M	Citric acid	1.0	99.4
	2-Amino BA	1.0	15.6
	Tetraethylenediaminetetraacetic acid	1.0	37.3
	Chloramine-T	1.0	66.4
	Dithizone	Saturate	78.5
	Sod. chromate	1.0	45.5
	Sod. metabisulphate	1.0	55.9
	Sod. dihydrogen phosphate	0.01	8.3
	Sod. dihydrogen phosphate	0.05	31.0
	Sod. dihydrogen phosphate	1.0	96.9
3 M	Disod. metaborates	1.0	36.5
	NaCl, $NaNO_3$, Na_2SO_4, $NaIO_3$	1.0	Activators
	Dithizone	0.25	21.1
	Dithizone	Saturate	47.5
	Polyvinylalcohol	Saturate	12.6

6.3. Corrosion inhibitor

The inhibition of the corrosion aluminum and its alloys in alkaline solution is well known and a number of inhibitors have already been described and investigated [75], they may be organic [76,77] or inorganic [78]. Using polarization method as well as weight loss method, Al-Suhybani et al. [79] studied various organic and inorganic inhibitor effects on the corrosion rate of aluminum in alkaline solution in detail. It was reported that various benzoin acid (BA) as well as other organic acids inhibit the corrosion but to different extents depending on the structure. The inhibition is due to the adsorption of these acids and not due to neutralizing effect. Effect of some organic and inorganic additive on the corrosion of Al in NaOH is shown in Table 5. Clearly, the citric acid shows a best inhibition at 5 M NaOH compared with other organic inhibitors. For inorganic inhibitors, dihydrogenphosphate are the best with an inhibition efficiency about 97.0%, while the others such as NaCl, $NaNO_3$, Na_2SO_4, $NaIO_3$ are activators.

Al-Suhybani et al. [79] reported that the inhibition efficiency depends on both the sodium hydroxide and the inhibitor concentrations. Increasing the sodium hydroxide concentration leads to a decrease in the inhibition efficiency, while the dependence on the inhibitor concentration is more complex. Fig. 16 shows the

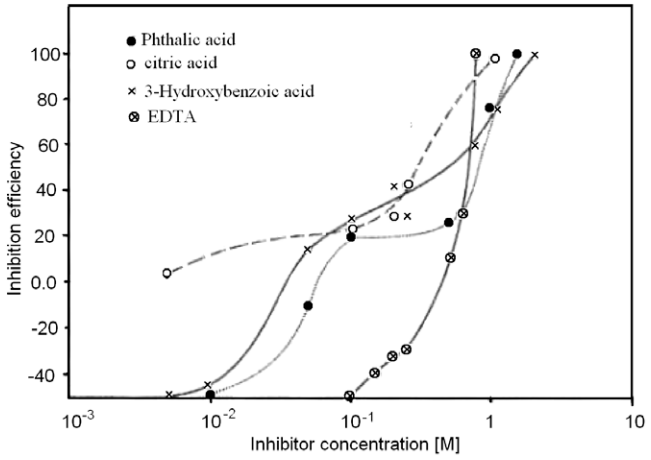

Fig. 16. Variation of inhibition efficiency with the concentration of some organic acids in 3 M NaOH [79].

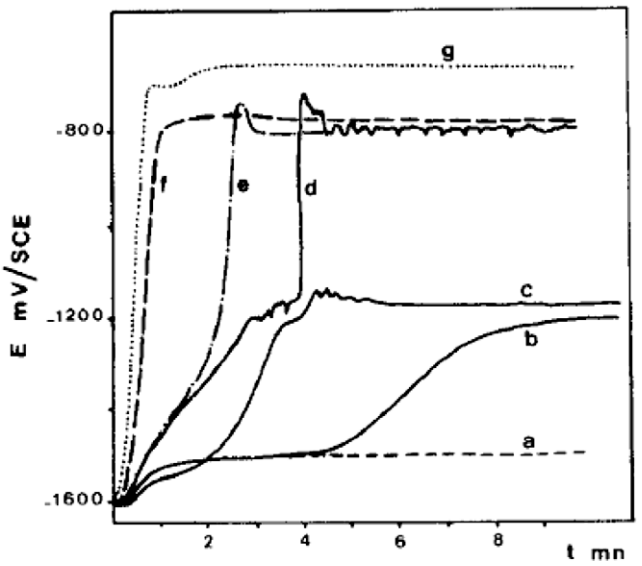

Fig. 17. Potential–time curves fro Almasilium alloys immersed in 0.1 NaOH solution at 60 °C, showing the effect of aluminate and 'silicate' ions: curve a, 0.1 N NaOH alone; curve b, 0.03 M Si; curve c, 0.04 M Si; curve d, 0.04 M Si + 0.0003 M A1; curve e, 0.04 M Si + 0.0006 M A l; curve f, 0.04 M Si + 0.0012 M A I; curve g, 0.04 M Si + 0.0018 M Al [80].

dependence of inhibition efficiency on concentration of several organic inhibitors. Clearly, the dependence is not linear. More specifically, the curve has a double-S shape for phathalic acid. The shape may indicate the formation of the second layer of adsorbed molecules. The figure also shows that phathalic acid and 3-hydroxy BA has stimulating effects at low concentrations while citric acid inhibits the corrosion even at low concentrations. The effect of ethylenediaminetetraacetic acid (EPTA) is also shown in the figure. The compound was found to be effective only at ~0.5 M. At low concentrations, it stimulates corrosion to the extent of ~90% at 0.01 M.

The sodium silicates have been found to be an effective inhibitor of corrosion in aluminum–alkaline systems [75, 80]. The inhibition is due to the formation of amorphous aluminosilicate film on the metal surface. It reported that a total and almost instantaneous inhibition can be obtained if both Si^{IV} and Al^{III} were presented in the solution. The same phase can be built up more slowly with silicate ions alone. The solution potential for different silicate concentration was also measured as function of time. The results are shown in Fig. 17. After an initial drop in the solution potential because of the dissolution of aluminum, the potential increases with time, followed by a series of oscillations that reveals a tendency for the inhibition film to become alternately partially or totally inhibiting [80]. Finally, the potential reaches a stabilization value. The larger the silicate concentration is, the greater the stabilization is as shown in the figure. Another effective inorganic inhibitor of corrosion of Al in alkaline solution is calcium tartrate which was studied by Shao et al. [81]. The authors reported inhibition efficiency >98% for the corrosion of pure aluminum in 1 M KOH solution. When the inhibitor concentration is low, its inhibition effect for the anodic process is much higher than that for cathodic process.

7. Summaries and conclusions

The current status of aluminum behavior in alkaline solutions, including the hydroxide equilibrium solid phases and the phase transition, prediction of aluminum solubility, organic and inorganic effects, aluminum corrosion and corrosion inhibition has been reviewed. This review should serve to aid the community engaged in the application of aluminum in engineering applications in the general knowledge of aluminum chemistry and corrosion and remind us to rethink some previous conclusions.

The solid hydroxide equilibrium phases play important roles in determining aluminum solubility. In general, the crystalline form of aluminum has a smaller aluminum solubility than amorphous form does. The phase transition is a complex function of operating conditions and the nature of materials utilized. In an alkaline solution, it is likely that the initial precipitates are always amorphous hydroxide which can be transformed into other forms of aluminum hydroxide by the action of water. At a specific operating condition, more-crystalline hydroxide is produced with aging. The crystallization process may be retarded, or the crystal habit of the precipitates may be changed by adding some organic or inorganic cation/anion such as citrate and boron. The retardation behavior is due to activity change at the solid/solution interface due to the adsorption of the adding anion/cation which leads to changes of the surface charge and interfacial tension and can influence the kinetics of the incorporation of the growth unit form the solution into the growing solid phase.

Aluminate ions ($Al(OH)_4^-$) is the only stable form of aluminum in an alkaline solution. The solubility is a function of solid hydroxide phases and increases with pH increasing. It is noted that some organics and inorganics can increase the aluminum solubility. The solubility can also be affected by the particle size presented in the solution. Nano particles are found in the solution and the particle size distribution is affected by the hydroxide phases and the adding organic elements.

Aluminum corrosion in alkaline solution is an electrochemical process. In a static solution, the corrosion rate decreases with exposure time. In a dynamic solution, the corrosion rates increase with increasing the flow velocity in mass transfer controlled regimes and dose not depends on flow velocity in active controlled regimes. The corrosion rate is influenced by adding organic and inorganic inhibitors into the alkaline solution or some other metal elements into the aluminum metal. The sodium silicates have been found to be an effective inhibitor with inhibition efficiency almost 100%.

Disclaimer

References

[1] S. Pyun, S. Moon, J. Solid State Electrochem. 4 (2000) 267.
[2] M. Klasky, M. Ding, J. Zhang, B.C. Letellier, D. Chen, Integrated chemical effects tests: Data analysis report and literature review, Report to Los Alamos National Laboratory, LA-UR-05-4881 (2005).
[3] R.S. Alwitt, in: J.S. Diggle, A.K. Vijh (Eds.), The Anodic Behavior of Metals and Semiconductors, vol. 4, 1974, p. 169.
[4] T.T. Foley, Corrosion 42 (1986) 277.
[5] S. Goldberg, J.A. Davis, J.D. Hem, in: G. Sposito (Ed.), The Environmental Chemistry of Aluminum, second ed., CRC Lewis Publisher, 1996, p. 271.
[6] A.R. Gerson, J.A. Counter, D.J. Cookson, J. Cryst. Growth 160 (1996) 346.
[7] H. Kodama, M. Schnitzer, Geoderma 24 (1980) 195.
[8] D. Nordstrom, H.M. May, in: G. Sposito (Ed.), The Environmental Chemistry of Aluminum, CRC Lewis Publisher, 1996, p. 39.

[9] A.C. Vermeulen, J.W. Geus, R.J. Stol, P.L. Debruyn, J. Colloid Interf. Sci. 51 (1975) 449.
[10] H.A. Van Straten, B.T.W. Holtkamp, P.L. Bruyn, J. Colloid Interf. Sci. 98 (1984) 342.
[11] M.K. Wang, J.L. White, S.L. Hem, Clays Clay Miner. 31 (1983) 65.
[12] P.L. Hayden, A.J. Rubin, in: Alan Rubin (Ed.), Aqueous Environmental Chemistry of Metals, Ann Arbor Science, 1976, p. 317.
[13] A.R. Gerson, Prog. Cryst. Growth Char. Mater. 43 (2001) 187.
[14] K.E. Hancock, G.E. Peck, D.L. Perry, J.L. white, S.L. Hem, J. Colloid Interf. Sci. 183 (1996) 431.
[15] C.J. Serna, J.L. white, S.L. Hem, J. Pharm. Sci. 67 (1978) 1179.
[16] K.P. Prodromou, Clays Clay Miner. 43 (1995) 111.
[17] G.C. Bye, J.G. Robinson, Kolloid-Zeitschr. Zeitschr. Polym. 198 (1964) 53.
[18] D.J. Aldcroft, G.C. Bye, C.A. Hughes, J. Appl. Chem. USSR 19 (1969) 167.
[19] P.J. Hsu, in: J.B. Dixon (Ed.), Mineral in Soil Environments, Soil Science Society of America, Madison, WI, 1989 (Chapter 7).
[20] S.L. Nail, J.L. White, S.L. Hem, J. Pharm. Sci. 65 (1976) 231.
[21] H. Li, J. Addai-Mensah, J.C. Thomas, A.R. Gerson, J. Cryst. Growth 279 (2005) 508.
[22] J.W. Mullin, Crystallisation, Butterwoth CRC Press, London, 1972. p. 207.
[23] P.H. Hsu, in: J. Nicholas (Ed.), Proceedings of the Third International Congress, Nice, France, 1973.
[24] G.M. Luciuk, P.M. Huang, Soil Sci. Soc. Am. Proc. 38 (1974) 235.
[25] M.F. Kwong, P.M. Huang, Soil Sci. Soc. Am. J. 41 (1977) 692.
[26] G.J. Ross, R.C. Turner, Soil Sci. Soc. Am. Proc. 35 (1971) 389.
[27] C.A. Beyrouty, G.E. Vanscoyoc, J.R. Feldkamp, Soil Sci. Soc. Am. J. 48 (1984) 284.
[28] F.J. Hingston, J.P. quirk, A.M. Posner, J. Soil Sci. 23 (1972) 177.
[29] J.R. Ferraro, J. Mol. Spectrosc. 4 (1960) 99.
[30] J.R. Feldkamp et al., J. Pharm. Sci. 70 (1981) 638.
[31] C.J. Serna, J.L. White, S.L. Hem, Soil Sci. Soc. Am. J. 41 (1977) 1009.
[32] L.H. Little, Infrared Spectra of Adsorbed Species, Academic Press, London, 1966.
[33] H.A. Van Straten, M.A.A. Schoonen, R.C.S. Verheul, Pl L. De Druyn, J. Colloid Interf. Sci. 106 (1985) 175.
[34] D. Langmuir, Aqueous Environmental Geochemistry, Grentice-Hall, Inc., 1997. p. 248.
[35] H. Baes, The Hydrolysis of Cations, Krieger Publishing Company, 1986.
[36] G.F. Vance, F.J. Stevenson, F.J. Sikora, in: G. Sposito (Ed.), The Environmental Chemistry of Aluminum, second ed., CRC Lewis Publisher, 1996, p. 169.
[37] A.E. Martell, R.J. Motekaitis, R.M. Smith, Polyhedron 9 (1990) 171.
[38] D. Dabbs, U. Ramachandran, S. Lu, J. Liu, L. Wang, I.A. Aksay, Langmuir 21 (2005) 11690.
[39] M.B. Shcihigol, N.B. Burchinskaya, J. Inorg. Chem. 4 (1961) 913.
[40] A.K. Babko, Russ. J. Inorg. Chem. 7 (1962) 1373.
[41] L.O. Ohman, S. Sjoberg, Mar. Chem. 17 (1985) 91.
[42] B. Tagirov, J. Schott, J.C. Harrichourry, J. Escalier, Geochim. Cosmochim. Acta 68 (2004) 1333.
[43] A. Douy, Solid State Sci. 7 (2005) 117.
[44] J. Simon, A. Vanderpol, E.J. Rerjerse, A.P.M. Kentgens, G.J. Vanmoorsel, E. Deboer, J. Chem. Soc. Faraday Trans. 90 (1994) 2663.
[45] K.P. Peil, L.G. Galya, G. Marcelin, J. Catal. 115 (1989) 441.
[46] F.J. Hingston, in: M.A. Anderson (Ed.), Adsorption of Inorganics at Solid–Liquid Interfaces, Ann Arbor Science Publishers Inc., Ann Arbor, Michigan, 1981.
[47] C.V. Toner, D.L. Sparks, Soil Sci. Soc. Am. J. 59 (1995) 395.
[48] C. Su, D.L. Suarez, Environ. Sci. Technol. 29 (1995) 302.
[49] P.A. Jordan, N.J. Clayden, S.L. Heath, G.R. Moore, A.K. Powell, A. Tapparo, Coordin. Chem. Rev. 149 (1996) 281.
[50] F.T. Bingham, in: Methods of Soil Analysis, Part 2, second ed., American Society of Agronomy, Madison, WI, 1982.
[51] W. Stumm, R. Kummert, L. Sigg, Croat. Chem. ACTA 53 (1980) 291.
[52] S. Goldberg, Plant Soil 193 (1997) 35.
[53] S. Goldberg, H.S. Forster, E.L. Heick, Soil Sci. Soc. Am. J. 57 (1993) 704.
[54] T. Oja, J.G. DosRamos, R.W. Reed, in: T. Provder (Ed.), ACS Symposium Series, vol. 881, 2004, p. 231.
[55] H. Bale, W.V. Rausch, J. Chem. Phys. 40 (1964) 3391.
[56] J.M. Rousseaux, P. Weisbecker, H. Muhr, E. Plasari, Ind. Eng. Chem. Res. 41 (2002) 6059.
[57] S. Pyun, S.-M. Moon, J. Solid State Electrochem. 4 (2000) 267.
[58] D. Chu, R.F. Savinell, Electrochem. Acta. 36 (1991) 1631.
[59] O.R. Brown, J.S. Whitley, Electrochim Acta 321 (1987) 545.
[60] S.M. Moon, S.I. Pyun, Corrosion Sci. 39 (1997) 399.
[61] W. Wihelmsen, T. Arnesen, O. Hasvold, N.J. Storkersen, Electrochim. Acta 36 (1991) 79.
[62] M.R. Tabrizi, S.B. Lyon, G.E. Thompson, J.M. Ferguson, Corros. Sci. 32 (1991) 733.
[63] C.D.S. Tuck, J.A. Hunter, C.M. Scamans, J. Electrochem. Soc. 110 (1987) 2970.
[64] S.M. Moon, S.I. Pyun, J. Solid State Electrochem. 2 (1998) 156.
[65] G.T. Burstein, R.T. Cinderey, Corros. Sci. 33 (1992) 475.
[66] S.M. Moon, S.I. Pyun, Electrochim. Acta 44 (1999) 2445.
[67] A.Y. Chatalov, in: Atlas of Electrocheimcal Equilibria in Aqueous Solutions, NACE, Houston, TX, 1974, p. 173.
[68] M. Pourbaix, Atlas of Electochemical Equilibria in Aqueous Solutions, NACE, Cebelcor, Houston, 1974.
[69] V. Vujicic, B. Lovrecek, Surface Technology 25 (1985) 49.
[70] A.B. McKee, R.H. Brown, Corrosion 3 (1947) 595.
[71] Coninental Group Inc., Aluminum Alloys for Handling High-Purity Water, Lawrence Livermore report, UCRL-15459 (1982).
[72] D.D. Macdonald, K.H. Lee, A. Moccari, D. Harrington, Corrosion 44 (1988) 652.
[73] W. Wilhelmsen, T. Arnesen, T. Hasvold, N.J. Storkersen, Electrochimica Acta 36 (1991) 79.
[74] F. Balbaud-Celerier, F. Barbier, Journal of Nuclear Materials 289 (2002) 227.
[75] E. Triki, G. Daufin, J.P. Labbe, J. Pagetti, Werkstoffe und Korrosion 30 (1979) 259.
[76] M. Fisher, in: Proceedings of the third European Symposium on Corrosion Inhibitors, Ferrara, Universita Degli Studi di Ferrara, Ferara, 1970, p. 15.
[77] I.N. Putilova, S.A. Balezin, V.P. Barannik, Metallic Corrosion Inhibitors, Pergamon, Oxford, 1960. p. 121.
[78] I.A. Ammar, A.F. Nazmi, Corrosion Prevention and Control 9 (1962) 31.
[79] A.A. Al-Suhybani, Y.H. Sultan, W.A. Hamid, Mat. –wiss. U. Werkstofftech 22 (1991) 301.
[80] J.P. Labbe, J. Pagetti, Thin Solid Films 82 (1981) 113.
[81] H.B. Shao, J.M. Wang, Z. Zhang, J.Q. Zhang, C.N. Cao, Corroison 57 (2001) 577.